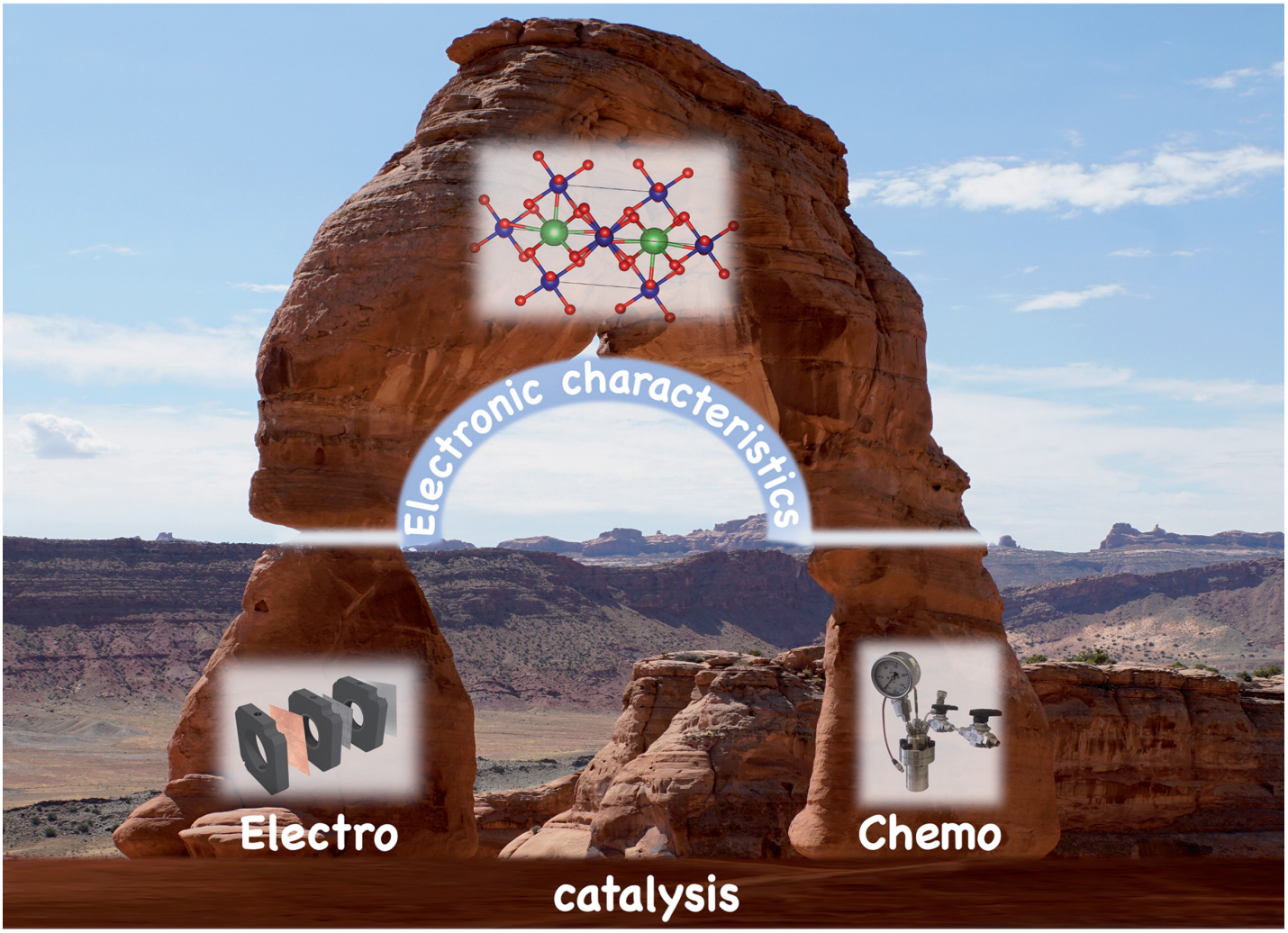

Showcasing research from Professor Regina Palkovits's laboratory, Institute for Technical and Macromolecular Chemistry, RWTH Aachen University, Germany.

Elucidating the validity of electronic characteristics of transition metal perovskites as descriptors bridging electro- and chemocatalysis

B-site substituted $LaCoO_3$ derivatives with perovskite-type structures were investigated in diverse electro- and chemocatalytic reactions to identify descriptors based on their electronic properties that are applicable across a wide range of reactions.

As featured in:

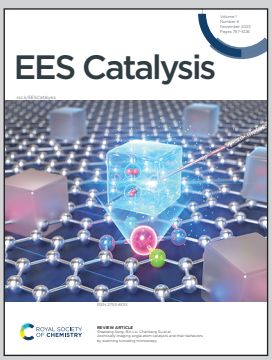

See Regina Palkovits *et al.*, *EES. Catal.*, 2023, **1**, 961.

ROYAL SOCIETY OF CHEMISTRY

rsc.li/EESCatalysis

Registered charity number: 207890

EES Catalysis

PAPER

View Article Online
View Journal | View Issue

Cite this: *EES Catal.*, 2023, 1, 961

Elucidating the validity of electronic characteristics of transition metal perovskites as descriptors bridging electro- and chemocatalysis†

Sonja D. Mürtz, ‡[a] Johannes Simböck, ‡[ab] Feng Zeng, [ca] Mahnaz Ghiasi,[d] Simon Schönebaum, [be] Ulrich Simon, [be] Frank M. F. de Groot [d] and Regina Palkovits *[ab]

Received 18th August 2023,
Accepted 28th August 2023

DOI: 10.1039/d3ey00206c

rsc.li/eescatalysis

The analysis of electronic characteristics as descriptors for the efficacy of catalysts provides fundamental insights into catalyst design criteria, but few studies address the applicability of descriptors across a broader range of reactions. This study on perovskite-type, B-site substituted $LaCoO_3$ derivates analyses the generalisability of the descriptor nature of electronic characteristics for electro- and chemocatalytic reactions – more specifically the occupancy of transition metal (TM) 3d orbitals, charge-transfer energy (CTE), and covalency in the interaction of O 2p – TM 3d states. The results show that among the analysed characteristics only covalency is a quasi-linear descriptor for the performance in electrocatalytic oxygen evolution reaction (OER), glycerol electro-oxidation reaction (GOR), as well as in five chemocatalytic reactions. The analysis of the reduction reaction of NO or N_2O by CO illustrates that not only reaction rates but also selectivity is determined by the same electronic catalyst characteristics. Measurement conditions in the analysis of electronic characteristics need to be chosen to recreate the oxidation state during the reaction-specific kinetically relevant step to yield adequate descriptor correlations. The results imply that significant synergies may be leveraged by enhanced collaboration across electro- and chemocatalysis research.

Broader context

Knowledge-based design of solid catalysts has been a long-standing challenge in catalysis research. Despite significant progress in structure–activity relationships through sophisticated experimental and computational methods, a holistic view of generalizable catalyst properties or even catalyst prediction has been elusive. The analysis of electronic characteristics as descriptors for the efficacy of catalysts provides fundamental insights into catalyst design criteria, but few studies address the applicability of descriptors across a broader range of reactions. This study on perovskite-type, B-site substituted $LaCoO_3$ derivates analyses the generalisability of the descriptor nature of electronic characteristics for electro- and chemocatalytic reactions. It focusses on the occupancy of transition metal (TM) 3d orbitals, charge-transfer energy, and covalency in the interaction of O 2p – TM 3d states. The results show that among the analysed characteristics only covalency is a quasi-linear descriptor for the performance in electrocatalytic oxygen evolution reaction, glycerol electro-oxidation reaction, as well as in five chemocatalytic reactions. The analysis of the chemocatalytic reduction reaction of NO or N_2O by CO illustrates that not only reaction rates but also selectivity is determined by the same electronic catalyst characteristics. The results imply that significant synergies may be leveraged by enhanced collaboration across electro- and chemocatalysis research.

[a] *Chair of Heterogeneous Catalysis and Chemical Technology, RWTH Aachen University, Worringerweg 2, 52074 Aachen, Germany. E-mail: palkovits@itmc.rwth-aachen.de*
[b] *Center for Automotive Catalytic Systems Aachen, RWTH Aachen University, Aachen, 52074, Germany*
[c] *State Key Laboratory of Materials-Oriented Chemical Engineering, College of Chemical Engineering, Nanjing Tech University, Nanjing, 211816, China*
[d] *Inorganic Chemistry and Catalysis, Debye Institute for Nanomaterials Science, Utrecht University, Universiteitsweg 99, 3584 CG Utrecht, The Netherlands*
[e] *Institute of Inorganic Chemistry, RWTH Aachen University, Landoltweg 1a, 52074 Aachen, Germany*

† Electronic supplementary information (ESI) available. See DOI: https://doi.org/10.1039/d3ey00206c

‡ These two authors contributed equally to this work.

Introduction

Efficient catalyst research for the screening of catalytic materials requires target characteristics of catalysts. Descriptors for those characteristics that ideally can be applied among several reactions and a variety of catalyst compositions are thus highly desirable to reduce experimental and computational effort.[1–3]

The descriptor nature of electronic characteristics for perovskite-type transition metal (TM) oxides has been discussed for many decades and is typically focused on the occupancy of TM

3d orbitals, split into t_{2g} and e_g orbitals.[4,5] Volcano-type or linear correlations of e_g and t_{2g} occupancy with performance have been reported for several different electrocatalytic reactions,[6–9] in particular the electrocatalytic oxygen evolution reaction (OER) on differently substituted perovskite-type oxides, as well as for chemocatalytic reactions, *e.g.* in flue gas abatement.[10,11] In addition, charge transfer energy (CTE) or bands near the Fermi-level and covalency have shown to be a descriptor in electro- and chemocatalysis,[10,12] respectively. In these catalytic applications, perovskite-type oxides are low-cost alternatives to platinum group metals because of their inherent activity[13] and vast compositional flexibility.[14] The latter underlines the need for catalyst design criteria to efficiently guide the search for catalysts with excellent performance in different reactions.

Recently, perovskite-type TM oxides have also gained increasing attention in the field of organic electrosynthesis,[15] where studies address the lack of fundamental knowledge on the electro-oxidation of alcohols on metal oxides, a potential alternative anode reaction in water splitting. The identification of reaction descriptors could accelerate the search for suitable materials, which is especially needed in the context of low-cost hydrogen production. To date, the literature about the electro-oxidation of alcohols is scarce. Although White,[16] Deshpande,[17] and Lan[18] have tested an impressive number of perovskite oxides for the electro-oxidation of methanol, there are few preliminary studies regarding higher alcohols. Lan *et al.*[18] investigated the electro-oxidation of ethanol on $LaRuO_3$ and $SrRuO_3$ and Dulce Morales *et al.*[19] and Santiago *et al.*[20] studied the performance of $LaNiO_3$ and $LaCoO_3$ in glycerol electro-oxidation reaction (GOR). However, no correlation of the performance with electronic properties was reported. Hence, the identification of structural and electronic descriptors is highly desired in this field and GOR is chosen as an example reaction in this study.

The B-site substituted perovskite-type oxides ($LaCo_{1-x}B_xO_3$, with B = Al, Ni, Zn) in this work have been used in a prior study, that introduced covalency in perovskite-type oxides as a descriptor for chemocatalytic reaction rates in NO oxidation, CO oxidation and N_2O decomposition.[11] Covalency was analysed by normalized quantification of the hybridized O 2p and TM 3d states as determined from X-ray absorption spectroscopy (XAS) at the O K-edge.[21] The descriptor nature of both t_{2g} and e_g occupancy as well as covalency has been interpreted as a measure for the electron transfer between active sites and reactants in the kinetically relevant step of the reaction and, thus, for the activation of the reactants. The correlation of TM 3d occupancy and covalency with surface-specific reaction rates depends on XAS measurement conditions as well. NO and CO oxidation rates correlated only with electronic characteristics measured in UHV-XAS when catalysts were partially reduced. In contrast, N_2O decomposition rates were linked to electronic characteristics of fully oxidized catalysts and did not yield any correlation with partially reduced catalysts. The limited scope of this previous work[11] motivated a look at a broader range of reactions.

This work uses the previously reported data on electronic characteristics to assess a broader scope of their use as descriptors towards correlations of electronic parameters with electrocatalytic performance in OER and GOR to bridge the fields of chemo- and electrocatalysis. Furthermore, it includes correlations with selectivity and surface specific reaction rates in the chemocatalytic reduction reactions of NO or N_2O by CO. Efficacy in all examined chemocatalytic reactions and the selectivity in the NO + CO reaction are quantified in steady state measurements for chemocatalysis, while overpotential, Tafel slope, and charge transfer resistance are determined for electrocatalytic efficacy. The effects of different catalyst composition and characteristics thus become apparent in the descriptor correlations, which are compared among all available reaction data spanning three electrocatalytic (including ORR from literature) and five chemocatalytic reactions (including three previously reported examples). The discussion of these correlations explores the generalisability of the descriptors and offers insights on possible knowledge transfer in catalyst design criteria between different reactions and fields of catalysis.

Results and discussion

Recapitulation of catalyst characteristics

The characteristics of the perovskite-type oxides used herein, with a composition of $LaCo_{0.8}X_{0.2}O_3$ (LCX-82), where X = Al, Ni, Zn, or $LaCo_{1-x}Al_xO_3$ with x = [0–0.8] ($LaCo_{0.8}Al_{0.2}O_3$ = LCA-82, for example), have been analysed in detail before: The electronic structure of the phase-pure perovskite-type oxides near the Fermi-level is generally dominated by contributions of O 2p as well as Co and Ni 3d states, in the catalysts at hand.[22,23] The non-TM cations La^{3+},[24] Al^{3+}[25] and Zn^{2+}[26] are of stable valence and do not contribute to the relevant density of states at this energy level. Electronic parameters were, thus, derived from analysis of respective TM $L_{2,3}$-edges and O K-edges, which were acquired in ultra-high vacuum (UHV) or in O_2 presence (0.37 kPa) at 623 K. The covalency factor was found to correlate with the CTE for the materials in this study. The analysis of the electronic parameters and their correlations are detailed in ref. 11 and summarized in Supplementary Notes 1–4 (ESI†).

Reaction-specific analysis of descriptors for single reactions

For the catalysts at hand, we present an analysis of the role of electronic parameters as descriptors for the performance in the electrocatalytic OER and GOR, as well as in the reduction reactions of N_2O or NO with CO. The results for N_2O decomposition as well as the reaction of NO or CO with O_2 have already been published[11] and are included in the final comparison of the descriptors of all aforementioned reactions.

Oxygen evolution reaction. We investigated the electrochemical performance of the obtained materials in a typical three electrode cell in a 1.0 M KOH solution. Despite a divergence in conditions between electrochemical measurements and XAS measurements, the electronic characteristics can be used for correlation with the electronic characteristics (see Supplementary Note 5 for more details, ESI†). The electronic parameters

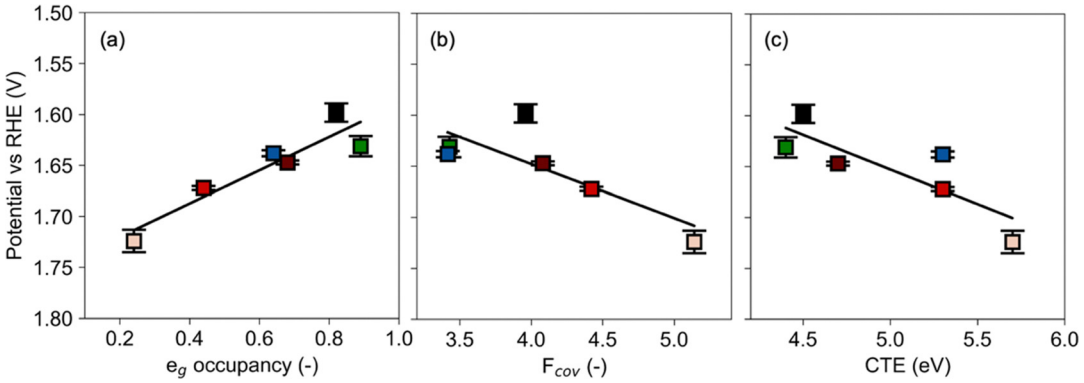

Fig. 1 The correlations between OER potential at 100 μA cm^{-2} with the e_g occupancy (a), covalency factor (b) and the CTE (c), respectively. The data and error were obtained based on three independent measurements. Ni (green), Zn (blue), increasing Al fraction (fading red fill) and LC (black). Lines represent least squares fits. (Electronic characteristics detailed in ref. 11.)

obtained in O_2 (fully oxidized, Co^{3+} ions) show a better correlation with OER performance than those acquired in UHV (partial Co^{2+} presence) because the oxides are expected to be fully oxidized in KOH solution under OER conditions (Supplementary Note 6, ESI†).

The OER potential at a current density of 100 μA cm^{-2} decreases linearly from 1.71 to 1.59 V *versus* reversible hydrogen electrode (RHE) with increasing e_g occupancy (Fig. 1a, details in Supplementary Note 7, ESI†). Perovskite-type TM oxides generally show a volcano shape in the correlation of OER activity and e_g occupancy, with a reported optimum at e_g occupancy = 1.2.[27] The materials at hand with an e_g occupancy lower than 1.2 thus appear on the left branch of this volcano plot. Moreover, both the Tafel slope and charge transfer resistance (R_{ct}) decrease with increasing e_g occupancy (Fig. S9, ESI†). All these correlations support the enhanced OER performance with increasing e_g occupancy in the investigated range. The volcano-type correlation has been interpreted in analogy to the Sabatier principle, which describes an ideal binding strength of reaction intermediates, *i.e.* neither too strong nor too weak.[27] In electrocatalysis, the intermediate reactant binding strength is amended by the capability of electron transfer that both take place in key reaction steps of the OER (Supplementary Note 9, ESI†).

In contrast to the correlation with e_g occupancy, the OER potential increases with increasing covalency (Fig. 1b). Abrishami *et al.* described a similar correlation of higher covalency factor and lower OER efficacy, citing degradation due to the oxidation of lattice oxygen at higher covalency.[28] The opposite trend of increasing OER efficacy with covalency factor has been reported for a series of $LaMO_3$, with (M = Mn, Co, Ni), which was ascribed to enhanced electron transfer.[29] A direct comparison of the work at hand to that study of non-substituted TM perovskites oxides is hampered by the effects of substitution in the LCAl materials. These conflicting reports may originate from a change in the OER mechanism as electronic characteristics vary, which has been shown for different values of CTE[12] (Supplementary Note 9, ESI†).

The OER potential at a current density of 100 μA cm^{-2} as well as Tafel slope and R_{ct} increases with increasing CTE from 4.4 to 5.7 eV (Fig. 1c and Fig. S9, ESI†), indicating sluggish kinetics. Interestingly, the catalytic performance to charge transfer correlation is less sensitive to the measurement conditions. In UHV, the potential also increases linearly with increasing CTE in analogy to literature reports,[12] indicating that CTE may be more suitable as a descriptor for OER. The lower efficacy in OER is observed as increasing CTE weakens the materials' ability to screen charge by introducing holes in O 2p band, thus decreases electron mobility to the surface and increases the necessity to adsorb OH^- to compensate charge at the interface.[12,30] With high CTE, the electron transfer is the rate determining step (RDS) due to the strong hydroxide affinity and slow electron transfer. As the CTE decreases, the rate determining step may shift to a concerted pathway because of the facilitated electron transfer and weakened hydroxide affinity. Further decreasing CTE leads to proton transfer as the RDS.[12] Concerning the catalysts in this study, the RDS may shift from an electron transfer step (LCA-82, LCZ-82, LCA-64, and LCA-28) to a concerted pathway (LCN-82 and LC) as the CTE decreases.

Glycerol oxidation reaction. The role of electronic parameters as descriptors for the performance in the electrocatalytic GOR is investigated in the same three-electrode setup with 1 M glycerol in 1 M KOH solution. Stronger correlations of the electrocatalytic performance were found with the parameters of the fully oxidized catalysts determined from XAS in O_2 presence which better matched the catalyst state under electro-oxidative conditions than data acquired in UHV. In addition, Oliviera *et al.*[31] demonstrated that Ni^{3+} plays a critical role as the catalytic active species in GOR. This insight combined with results from MeOH oxidation[32–34] on perovskites highlights the significance of high valence ions at the B-site for GOR and indicates that the fully oxidized state of the catalyst is crucial for accurate evaluation of its electrocatalytic performance. Fig. 2a depicts the correlation of the GOR potential at 100 μA cm^{-2} with the occupancy of the e_g orbitals, capturing the binding strength between catalyst surface and adsorbate sufficiently, although the metal–adsorbate interaction can be further enhanced through π-back donation involving t_{2g} states.[7] The GOR performance is enhanced by increasing e_g

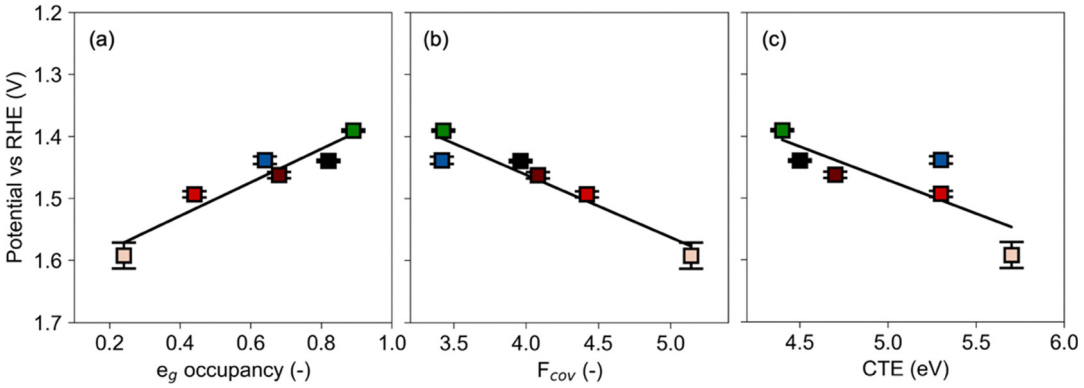

Fig. 2 The correlations between GOR potential with the e_g occupancy (a), covalency factor (b) and the CTE (c), respectively. The data and errors were obtained based on three independent measurements. Ni (green), Zn (blue), increasing Al fraction (fading red fill) and LC (black). Lines represent least squares fits. (Electronic characteristics detailed in ref. 11.)

occupancy as the used catalysts are located in the left branch of a volcano plot according to the Sabatier principle described above.

The metal–oxygen covalency determines the ability of the active site to interact with surface species during the kinetically relevant step. It is particularly considered as a descriptor when lattice oxygen participates in the reaction mechanism *via* the Mars–van-Krevelen mechanism because e_g filling is not an accurate descriptor in this case.[12] The ability of the active site to interact is important for the mechanism as the following steps are proposed for CO oxidation: Adsorption of CO on the B-site takes place, followed by the reaction of adsorbed CO with the lattice oxygen forming CO_2 and leaving a positively charged oxygen vacancy in the lattice. Further, the hydroxyl ions from the electrolyte are attracted by the oxygen vacancy, retaining the surface structure of the perovskite.[15] Although further research is needed to fully understand the mechanism of GOR on perovskite oxides, studies on CO oxidation suggest that lattice oxygen may also play an active role in oxidizing adsorbed methoxy groups of organic substrates.[35–37] Therefore, high oxide ion and vacancy mobility is desirable. The thermodynamics of the oxygen vacancy formation and mobility are influenced by the position of the Fermi level, which is decreased by a more electronegative metal on the B site. Conversely, increasing the electron density in Co–O by Al substitution decreases the GOR performance with increasing covalency, as shown in Fig. 2b. Moreover, the efficiency of electrocatalytic reactions is strongly affected by the electron transfer barrier. Hence, the CTE is an important descriptor of electrocatalytic performance in GOR because it reflects the ease with which electrons can be transferred between the catalyst and the reactants. A lower CTE means that electrons can more easily transfer from the catalyst to the reactants, leading to faster reaction rates and higher catalytic efficiency as mentioned above. This study demonstrates that decreased CTE promotes electrocatalytic performance in GOR as shown in Fig. 2c, complementing the results from OER in the previous section. Tafel slope and R_{ct} follow the same trend as the GOR potential for all three electronic parameters (see Fig. S10, ESI†).

N_2O + CO reaction. The reduction reaction of N_2O by CO selectively yields the products N_2 and CO_2. The impact of reaction steps from N_2O decomposition is insignificant because reaction temperatures were below the threshold of N_2O decomposition activity in tests of the same catalysts.[11] The N_2O + CO reaction rate increases linearly with higher t_{2g} and lower e_g occupancy but only when the electronic parameters are derived from XAS in O_2 presence, when the catalysts are fully oxidized (Fig. 3a and b). The covalency factor in fully oxidized catalysts is a similarly adequate linear descriptor for increasing reaction rates as well (Fig. 3c). These results are analogous to correlations of the N_2O decomposition rate with the same electronic parameters.[11] The correlation of reaction rates with characteristics of the oxidized catalysts indicates an oxidizing interaction during the kinetically relevant activation of N_2O in the reaction with CO*. The mechanistic analysis (see Supporting Note 11, ESI†) elucidated that the kinetically relevant step involves a facilitated activation of adsorbed N_2O* (O η^1) on TM sites. In this binding environment the N–O bond weakens with an increased transfer of electron density from TM states into the anti-bonding lowest unoccupied molecular orbital (LUMO) of the N_2O molecule, which transitions from linear into bent geometry[38] (Fig. 4a). The withdrawal of electron density from the catalyst reflects the oxidizing interaction during the kinetically relevant step, where CO_2* is the remaining product on the surface, typically adsorbed as electron density withdrawing carbonate.[39] Thus, the mechanistic analysis agrees well with the result that correlation of N_2O and CO reaction rates with electronic characteristics are only valid when measured of the fully oxidized catalysts.

NO + CO reaction. Details of the NO + CO reaction, which yields CO_2 and N_2 or N_2O as products, on perovskite-type oxides have been the subject of several studies as reviewed by Royer *et al.*[13] In general, the selectivity branching point between N_2 or N_2O adds complexity to the analysis of the NO + CO reaction compared to the N_2O + CO reaction.[40] In this work, the choice of reaction conditions at 523 K allows to disregard any consecutive reaction of N_2O to N_2 because conversions for both N_2O decomposition and the reduction of N_2O by CO were below

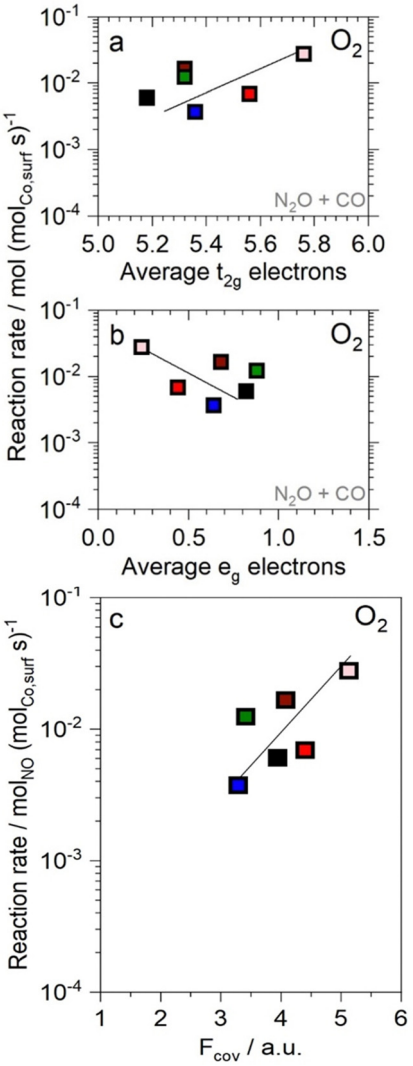

Fig. 3 Correlation of N_2O + CO reaction rates at 603 K with (**a**) t_{2g} electrons (b) e_g electrons and (**c**) covalency. Ni (green), Zn (blue), increasing Al fraction (fading red fill) and LC (black). Lines represent least squares fits. (Electronic characteristics detailed in ref. 11).

5% at conditions below 573 K on the catalysts at hand. It should be noted, however, that any comparison to reaction measurements at elevated temperatures needs to consider consecutive/parallel reactions, which cause a shift towards N_2 selectivity as reported in several studies.[13] Furthermore, isocyanate (NCO^-) surface species are unreactive in the reaction conditions applied here.[41] Mechanistic analysis shows that the disproportionation reaction of two NO molecules is not a major pathway to form N_2O under the reaction conditions applied here (see Supporting Note 11, ESI†). As a result, the reaction of two adsorbed N atoms (eqn (S12), ESI†) remains the only N_2 formation pathway under the applied reaction conditions, whereas N_2O forms in a parallel reaction of N* and NO* (eqn (S11), ESI†).

The ratio of product formation rates of N_2O/N_2 in the NO + CO reaction correlates with the electronic parameters of the fully oxidized catalysts (Fig. 5a–c): N_2 selectivity decreases with increasing covalency and t_{2g} orbital occupancy, while it increases with e_g occupancy. Analysis of the origin of this effect of electronic parameters on the selectivity requires a comparison of the competing reaction steps in the formation of N_2 or N_2O and the respective interaction of active site and reactant. The N_2O formation in the reaction of N* with NO* involves the activation of the NO* molecule. This activation is facilitated by electron transfer into the anti-bonding LUMO of the NO molecule through t_{2g} π-interactions, which weaken the N–O bond (Fig. 4c).[42] The TM e_g orbitals of the active site of the catalyst also interact with the NO molecule *via* σ-interaction, wherein electron density is transferred from the bonding $2\sigma_g$-bond of the NO molecule. In contrast, the formation of N_2 in the reaction of two N* atoms with N 2p orbital character does not involve comparable activation through the interaction with t_{2g} and e_g orbitals of the TM. Thus, the selectivity towards N_2O increases with elevated covalency, which is a descriptor for potential electron transfer from the active site into the NO* molecule.

The correlation of the selectivity ratio with electronic characteristics of the fully oxidized catalysts is an indication that the active site of the catalyst is oxidized or in an oxidized state during the decisive interactions with reactants in the relevant elementary steps, N* and NO* (Scheme S2, ESI†). The electronegative N* is highly electrophile and thus may act partially oxidizing analogously to oxygen species. NO* is partially electron withdrawing in nature as described above for its activation, as the electron transfer into the anti-bonding LUMO leads to the formation of an NO^- species.[42] The oxidizing nature of the reactants in the relevant elementary steps thus leads to the necessity of measuring electronic characteristics on fully oxidized catalysts.

In remarkable contrast to the selectivity correlations, the overall reaction rate in the NO + CO reaction correlates only with the electronic characteristics analysed for the partially reduced catalysts (Fig. 5d–f). The correlations with t_{2g} and e_g in volcano-type plots and the linear increase of the reaction rates with covalency in UHV are analogous to results for NO or CO oxidation reaction rates.[11] This finding indicates that in this reaction pathway, a partially reduced active site is present during the kinetically relevant step, *i.e.* the surface reaction of NO* and CO* (see analysis in Supplementary Note 11, ESI†). The TM surface site is in a partially reduced state during the interaction with the adsorbed electron-donating CO molecule, similar to the case in CO oxidation.[11] The correlations with the electronic parameters are valid for partially reduced catalysts only, despite the typically oxidizing effect of NO, which appears to be superseded by the reducing effect of CO in the corresponding transition state of the surface reaction. The present analysis of oxidation states *via* XAS in UHV and O_2 presence does not allow sufficient insight to discern the effects of adsorbed reactants on surface oxidation states of the catalysts, meriting future investigation of the catalyst state in the presence of different reactant gases in *in situ* XAS measurements.

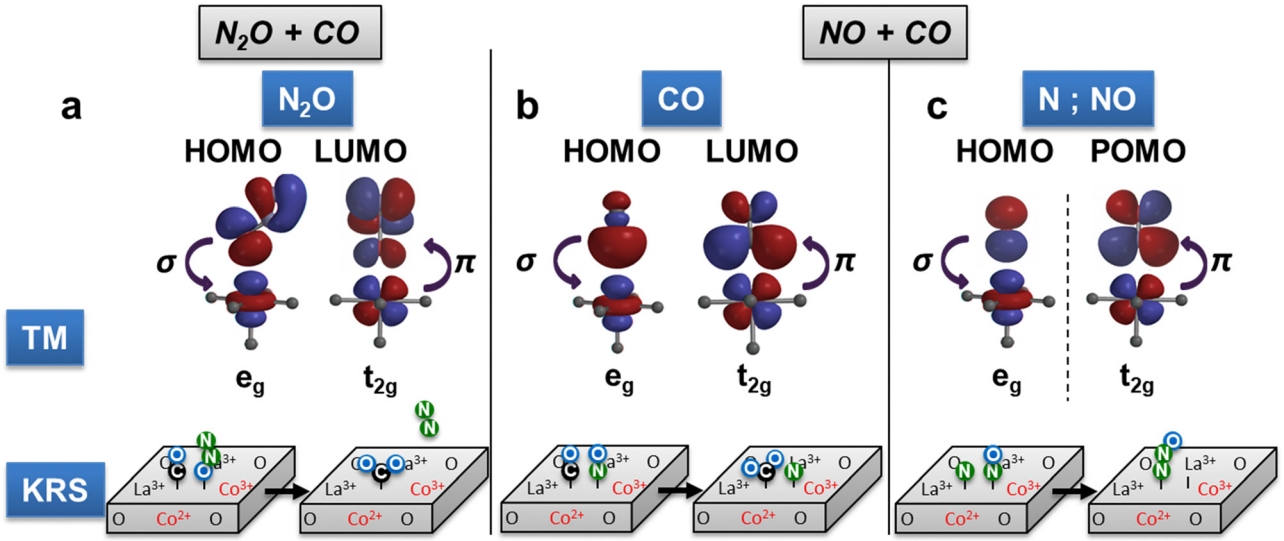

Fig. 4 Interaction of reactants with the catalyst surface in N_2O and NO reduction by CO. Interaction of frontier orbitals of the transition metal (TM) and surface species. (a) N_2O + CO reaction. (b) NO + CO reaction selectivity (c) NO + CO reaction rate. The schematics at the bottom show the kinetically relevant step (KRS) of the respective reaction. Please note that the schematic does not include the complexity of binding sites on the catalyst.

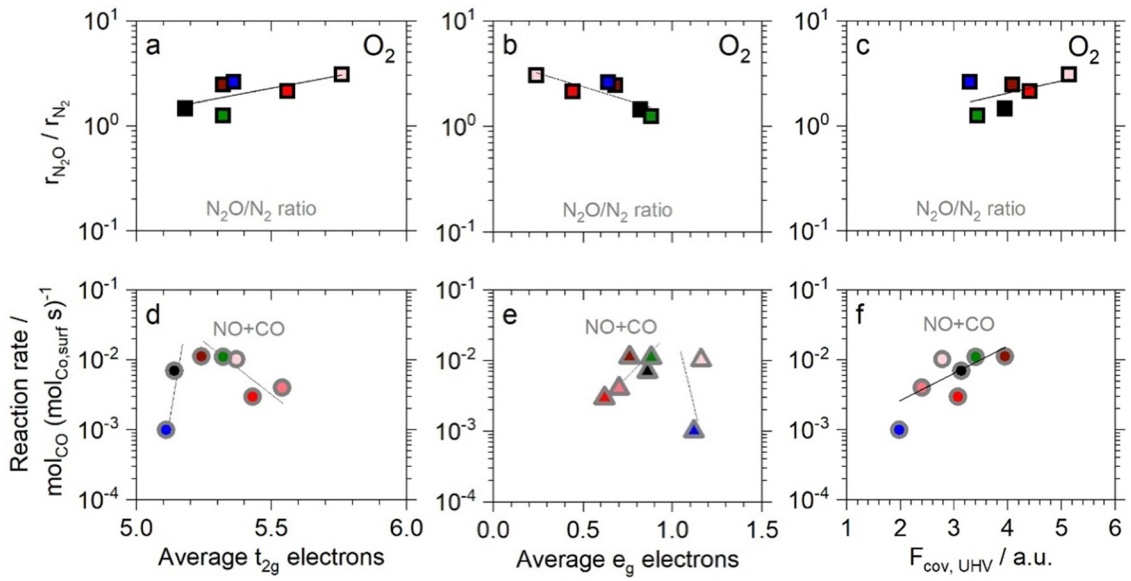

Fig. 5 Correlation of NO + CO product selectivity and reaction rates, all at 523 K, with electronic characteristics: (a) and (d) t_{2g} electrons, (b) and (e) e_g electrons and (c) and (f) covalency factor. Symbol edge color identifies F_{cov} in O_2 presence (black) or UHV (gray). Ni (green), Zn (blue), increasing Al fraction (fading red fill) and LC (black). Lines represent least squares fits. (Electronic characteristics detailed in ref. 11.)

Descriptors for different reactions – parallels and differences

In the first part of this work, correlations between electrocatalytic performance and electronic parameters have been analysed for OER and GOR. The results confirm that the electrocatalytic activity of the TM-based perovskite-type oxides can be described by e_g occupancy, covalency, as well as CTE (see Table 1). Electrocatalysis involves electron transfer in the catalyst material as a potential is applied. The ease of electron transfer in the catalytic material increases with lower CTE, as this is the energy required for the electron transfer of O 2p states in the valence band to Co 3d states in the conduction band. At low CTE values activity reportedly becomes quasi-independent of it, but no catalyst in this work is below this threshold.[12] As both electron transfer and molecular activation of the reactants are relevant for the catalysts at hand both covalency and CTE are descriptors in OER and GOR. However, literature on ORR surprisingly reports no performance correlation with CTE, but only with e_g occupancy and covalency.[43,44] The latter can even be extended to CO_2 reduction and hydrogen evolution.[45]

Table 1 Overview on viable correlations of e_g or t_{2g} occupancy, covalency, and CTE in the investigated reactions. Green, yellow, and red mark linear, volcano-type, and no correlation, respectively

		Catalyst state	e_g or t_{2g} occupancy	F_{cov} (Covalency)	CTE
Electrocatalysis					
OER	This work and ref	Oxidized	✓ (e_g)	✓ [27,28]	✓ [12]
GOR	This work	Oxidized	✓ (e_g)	✓	✓
ORR	Ref	—	✓ (e_g) [46]	✓ [46]	✗ [44]
Chemocatalysis					
NO oxidation	Ref. 11	Part. reduced	✓ (e_g+t_{2g})	✓	✗
CO oxidation	Ref. 11	Part. reduced	✓ (e_g+t_{2g})	✓	✗
N_2O decomposition	Ref. 11	Oxidized	✓ (e_g+t_{2g})	✓	✗
N_2O + CO	This work	Oxidized	✓ (e_g+t_{2g})	✓	✗
NO + CO	This work	Part. reduced	✓ (e_g+t_{2g})	✓	✗
NO + CO selectivity	This work	Oxidized	✓ (e_g+t_{2g})	✓	✗

The chemocatalytic results illustrate that catalytic efficacy in terms of reaction rates can be described for the reduction reactions of NO or N_2O with CO. This finding amends the conclusions of a previous study on the reactions of NO and CO with O_2, as well as N_2O decomposition,[11] that a broad set of reactions may be described by the same electronic parameters. The linear relationship for OER and GOR performance contrasts with that observed for the chemocatalytic reaction rates. This discrepancy can be attributed to the different performance metrics, where chemocatalytic reaction rates are normalized by surface sites in contrast to electrochemical overpotential. The calculation of active surface sites, as described in previous work,[11] involves the BET surface area, the TM content derived from XRF measurements, and particularly the approximation of the number of Co atoms per nm^2 at the catalyst surface based on the geometry of the $LaCoO_3$ 001 facet. While this is a good first approximation, because the 001 facet of $LaCoO_3$ is the most stable, this approach neglects the real distribution of facets that will differ among the catalyst materials. Overall, the derived value of surface sites – and its unknown variance – factors in as the denominator in the calculation of the surface specific chemocatalytic reaction rates and thus has significant impact on the resulting reaction rate – causing deviation from linear correlations. The results show that the correlation is valid despite the applied approximations, though the latter lead to more significant scatter. Future work should be dedicated to improve the determination of active surface sites and, thus, the accuracy of the correlations.

The covalency factor is most adequate among the studied electronic parameters as a descriptor for chemocatalysis (Table 1). The results highlight the significant link between the mechanism of a chemocatalytic reaction and the electronic characteristics of the catalyst as reducing or oxidizing interactions of the catalyst and the reactants during the kinetically relevant step have to be recreated in order to obtain valid correlations. The results of this and previous work separate two groups of reactions (Fig. 6): Catalytic rates in NO oxidation, CO oxidation, and NO reduction by CO are linked to characteristics of partially reduced catalysts, while catalytic rates in N_2O decomposition and N_2O reduction by CO as well as the selectivity in the NO + CO reaction depend on characteristics of fully oxidized catalysts.

Significantly, the results on selectivity in the NO + CO reaction show that the electronic parameters can serve as a

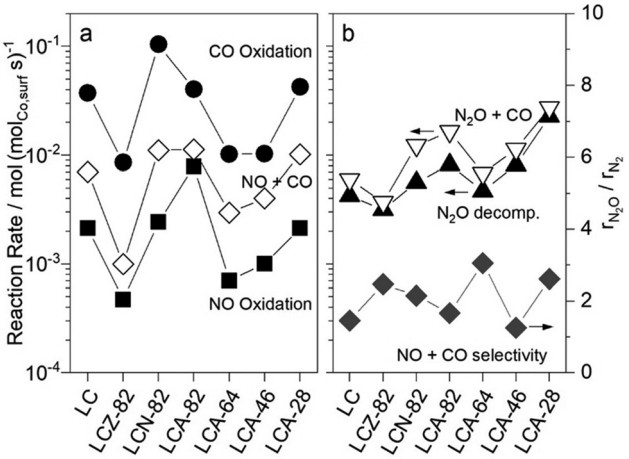

Fig. 6 Trends of catalytic efficacy of catalysts. (a) Reaction rates in NO oxidation at 523 K, CO oxidation at 443 K and NO + CO reaction at 523 K. (b) N_2O + CO and N_2O decomposition reaction rates at 603 K and 673 K, respectively as well as NO + CO selectivity at 523 K.

descriptor for selectivity. The ability to apply the same set of descriptors to both reaction rate and selectivity of a chemocatalytic reaction allows for conclusions on catalyst design and the suitability of TM-based perovskite-type oxides for the NO + CO reaction: The desired characteristics for high reaction rates differ significantly from those for the desired selectivity at low temperatures. The reaction rate increases with more pronounced covalency while the selectivity shifts towards undesired N_2O at high covalency values – an apparent inherent trade-off in the catalyst design. Thus, catalyst design of perovskite oxides must follow a middle ground in terms of covalency to optimize the overall catalyst performance at low temperatures, which complicates an effective use of these catalysts in this reaction.

A major difference in the results of electro- and chemocatalytic reactions, however, is the performance of CTE (Table 1), which is a descriptor for efficacy in OER and GOR but not in any chemocatalytic reaction in this work. This finding may reflect the differences between electro- and chemocatalysis. Chemocatalysis depends on the activation of the reactant on the catalyst surface, while electrocatalysis involves electron transfer from the catalyst to the reactant in addition to the interaction on the surface. Furthermore, the descriptor nature of e_g occupancy and particularly covalency in both electrocatalysis and chemocatalytic reactions may allow for synergy in material research for chemo- and electrocatalysis.

The fundamental nature of the interaction of catalyst and reactants implies that the used electronic parameters may be applicable for an even wider range of reactions. Hence, a one-time analysis of the parameters can deliver the relative efficacy of a set of catalysts for many reactions at once. Overall, these findings merit further analysis of the descriptors shared among chemo- and electrocatalysis.

In addition, the results of all reactions emphasize how significant the choice of XAS reaction conditions is for the applicability of descriptors: Reaction rates and selectivity in the NO + CO reaction were acquired in the same steady state measurements, *i.e.* a steady overall catalyst state was present. In NO + CO reaction conditions the catalyst is reported to be generally slightly reduced overall.[47] Hence, a conclusion could be that a partially reduced catalyst state should be able to deliver descriptors for all important aspects of the reaction. Yet, this conclusion proved incorrect as selectivity correlates with oxidized catalysts. This result emphasizes that an oxidizing or reducing catalyst–reactant interaction in the kinetically relevant step determines the adequacy of XAS measurement conditions. The observed strong dependence on XAS measurement conditions in chemocatalytic reactions is analogous but less pronounced in OER and GOR. The results illustrate as well that careful consideration of experimental conditions for *in situ* analysis – in XAS or other characterisation techniques – is needed to analyse catalyst characteristics adequately. Furthermore, as the necessary measurement conditions may differ for separate aspects of an individual reaction, *i.e.* reaction rates and selectivity, emphasis rests on the identification of the corresponding kinetically relevant steps. Mechanistic aspects and the characteristics of the active site during the kinetically relevant step thus are of vital importance for an informed choice of pre-treatment and *in situ* measurement conditions for XAS or any other *in situ* catalyst characterisation technique. Likewise, past measurements should be scrutinized towards their experimental parameters when descriptors for catalyst performance are discussed.

In summary, insights are yielded not only on the reaction mechanism but also on the nature of the catalyst–reactant interaction and consequences for the analysis of catalyst characteristics and descriptors in general. The approach shown here generally requires a structural interaction of transition metal cations with oxide, other anions or ligands because it exploits the TM-ligand covalency as descriptor for the catalytic interaction. It is thus applicable for most TM-based compounds, such as TM oxides and their various structures, spinels for example. It further applies to other TM-based compounds, such as sulfides or nitrides. The approach shown here may be applicable to material systems of single atom catalysts, depending on their exact composition. It may shed light on the nature of active site–support interaction in systems such as Pt_1/FeOx for example. These results on reaction mechanism and adequate analysis of descriptors show that further analysis of such correlations can profoundly contribute to the understanding of catalyst performance. Synergies are likely to emerge with density functional theory (DFT) modelling of catalyst–reactant interactions for the analysis of reaction mechanisms, in a way that DFT modelling may predict the adequate XAS measurement conditions. A combined application of electronic parameters and DFT calculation of reactant–catalyst interaction may support catalyst research and targeted catalyst design significantly, in particular if the correlations presented here can be confirmed for other TM oxide structures.

Further insights on the reaction mechanisms may be provided, if reaction-specific XAS measurement conditions are applied to analyse catalyst characteristics in the presence of the respective reactants, surface species, and oxidation states.

Experimental

The catalyst synthesis method *via* a citrate route and information on the analysis of the catalysts *via* X-ray fluorescence, X-ray diffractometry, N_2-physisorption and X-ray absorption spectroscopy measurements have been detailed elsewhere.[11] The procedure of catalyst preparation for measurements, details on catalytic reaction measurement and the setup used therein is also available in ref. 11.

Electrochemical oxygen evolution and glycerol oxidation were performed with an Autolab PGSTAT 302 N electrochemical workstation connected to a three-electrode cell with a glassy carbon rotating disc as the working electrode, an Ag/AgCl electrode as the reference electrode, and a glassy carbon rod as the counter electrode. Cyclic voltammetry (CV) and electrochemical impedance spectroscopy (EIS) measurements were performed to obtain the overpotential, current density, Tafel

slope, and electrochemically active surface area (ECSA). More details can be found in Supplementary Note 10 (ESI†).

Chemocatalytic reaction rate measurements were conducted in steady state conditions and measurements, which were repeated at the same experimental conditions to provide information on deactivation or activation of the catalyst. If applicable, the change in catalytic rate over time was corrected by linear interpolation. The obtained reaction rates are surface specific after normalization to the Co and Ni content in the catalyst and the catalyst surface area as determined *via* the Brunauer–Emmett–Teller method from N_2-physisorption. As conversion increases along the catalytic bed, reactant concentrations differ from inlet conditions. The effect of this change in partial pressure was approximated by calculating the mean of the reactor bed inlet and outlet concentration. This mean partial pressure was used for presentation of the effect of partial pressures on reaction rates and selectivity in the ESI.†

Details on the used gases in reaction measurements are provided in Table S3 (ESI†). Inlet reactant partial pressures for the reactions in this work were 0.21 kPa NO, 0.21 kPa CO and 0.19 kPa N_2O, when they were not varied in measurements for the effect of partial pressure on catalytic rates. N_2O and N_2 were not co-fed in reaction rate measurements for the NO + CO reaction. The selectivity values were determined by measurement of N_2O and forming the N-balance from NO inlet and measured N_2O concentration to yield the selectivity to N_2. In the mechanistic model presented in this work, the formation of each N_2O molecule consumes a NO molecule that is not activated in the kinetically relevant step. Accordingly, the reaction rate data, which should reflect the NO molecules as consumed in the kinetically relevant step, was calculated from the experimental reaction rate and the measured selectivity towards N_2O.

Conclusions

In this work the generalisability of the descriptor nature of electronic characteristics was investigated on the basis of Co-based perovskite-type oxides. Correlations of the occupancy of transition metal (TM) 3d orbitals, charge-transfer energy (CTE), and covalency in the interaction of O 2p and TM 3d states are compared among two electrocatalytic and five chemocatalytic reactions including results of previous work.

The obtained correlations of all reactions emphasize the importance of the choice of XAS reaction conditions for the applicability of descriptors. In electrocatalysis, the materials' catalytic performance for the oxygen evolution reaction (OER) and glycerol oxidation reaction (GOR) correlates better with the electronic parameters obtained in O_2-containing atmosphere indicating the fully oxidized states of the materials play a key role in these reactions. The overpotential, as well as the Tafel slope, and charge transfer resistance decrease linearly with increasing e_g occupancy, while they increase with increasing covalency factor and CTE. These trends appear for both reactions underlining the applicability of the descriptors.

The presented results of the chemocatalytic reactions broaden the evidence that covalency in Co-based perovskite-type oxides is a highly relevant descriptor for reaction rates. The initial mechanistic analysis of the reduction of NO or N_2O by CO concludes that a CO-assisted step is the likely kinetically relevant step in either of N_2O and NO reduction by CO. The correlations of reaction rates and selectivity with electronic parameters however depend on the state of the catalyst during the analysis of electronic characteristics as reactions correlate with data from fully oxidized or partially reduced catalysts. NO + CO reaction as well as NO and CO oxidation rates relate to characteristics of partially reduced catalysts, while N_2O decomposition and N_2O reduction by CO are linked to fully oxidized catalysts. This dependence is based on the electronic characteristics during the kinetically relevant elementary steps as the active site interacts with the reactants.

In addition, the descriptor nature of covalency has been shown for selectivity in the NO + CO reaction in absence of N_2O reactivity: The selectivity towards N_2O relative to N_2 increases with covalency. This also results in an inherent trade-off between overall catalytic rates and desired selectivity towards N_2 at low temperatures. The correlations of t_{2g} and e_g occupancy or covalency with the selectivity in the NO + CO reaction are only valid for fully oxidized catalysts, while the reaction rate correlates with partially reduced catalysts. This is a remarkable difference due to different elementary steps determining reaction rates and selectivity within the NO + CO reaction. The interaction with different reactants in these elementary steps causes different oxidation states of the catalyst to be relevant. This result renders *in situ* characterisation of catalysts for the NO + CO reaction yet more complex because reaction rates and selectivity cannot be described by measurements in a single catalyst state. This complexity may apply for *in situ* characterisation of other reaction systems than the NO + CO reaction on Co based perovskite-type oxides as well – depending on the individual reaction mechanism on the catalyst.

Overall, the variety of reactions bridging electro- and chemocatalysis illustrates that covalency is a broadly applicable descriptor for the performance of perovskite-type TM oxides proving its generalisability from electrocatalytic oxygen evolution and reduction, over organic electro-oxidation, to chemocatalytic reductions and oxidations of NO, CO, as well as N_2O decomposition. The results show that considerable synergies can be exploited through increased cooperation between electrocatalysis and chemocatalysis research.

Author contributions

J. S., F. Z., S. M., F. G. and R. P. conceived the idea of this work. R. P. supervised the work. S. M. and F. Z. guided or performed the electrocatalytic measurements as well as the respective data analysis. J. S. guided or performed chemocatalytic reaction rate measurements as well as the respective data analysis. F. G. and M. G. advised on the analysis of XAS data and their interpretation. S. S. and U. S. contributed XRF experiments and analysis.

S. M., J. S. and F. Z. wrote the manuscript; all authors discussed the results and contributed to the improvement of the manuscript.

Conflicts of interest

There are no conflicts to declare.

Acknowledgements

This work is part of the project house ''Center for Automotive Catalytic Systems Aachen – ACA'' of RWTH Aachen University and supported by the Cluster of Excellence Fuel Science Center (EXC 2186, ID: 390919832) funded by the Excellence Initiative by the German federal and state governments to promote science and research at German universities. This study was conducted in connection to the project ''Digitalization in Catalysis'' NFDI4Cat – ID: 441926934 funded by German Research Foundation (DFG). This research used resources of the Advanced Light Source, which is a DOE Office of Science User Facility under contract no. DE-AC02-05CH11231. The authors are grateful for the support received from the team of beamline 11.0.2 at the ALS, particularly by Dr Hendrik Bluhm and by James Wu (LBNL) for sample preparation for XAS analysis. The authors thank Dr David Müller (FZ Jülich) for providing the data for XAS experiments on gaseous O_2 in front of an Au foil. J. S. thanks the German Academic Exchange Service (DAAD) for financial support through the thematic network ACalNet. S. M. acknowledges funding by Cusanuswerk e.V. The authors acknowledge assistance in catalyst synthesis by Jil Schosseler, B.Sc. (RWTH Aachen University), and in several reaction rate measurements by Steffen Feldhues B.Sc. (RWTH Aachen University), Dr Dilek Varisli, and M.Sc. Edison Zuluaga (Both UC Berkeley). J. S. thanks Prof. Enrique Iglesia (UC Berkeley) for financial support and discussions in preparation of and during the measurements at the ALS.

References

1 J. Wu and Y. X. Yu, *Catal. Sci. Technol.*, 2021, **11**, 7160–7170.
2 J. Wu and Y. X. Yu, *J. Colloid Interface Sci.*, 2022, **623**, 432–444.
3 J. H. Li and Y. X. Yu, *ChemSusChem*, 2021, **14**, 5488–5498.
4 R. J. H. Voorhoeve, D. W. Johnson, J. P. Remeika and P. K. Gallagher, *Science*, 1977, **195**, 827–833.
5 B. Viswanathan, *Catal. Rev.*, 2006, **34**, 337–354.
6 Deeksha, P. Kour, I. Ahmed, Sunny, S. K. Sharma, K. Yadav and Y. K. Mishra, *ChemCatChem*, 2023, **15**, e202300040.
7 J. Suntivich, K. J. May, H. A. Gasteiger, J. B. Goodenough and Y. Shao-Horn, *Science*, 2011, **334**, 1383–1385.
8 Y. Abe, I. Satoh, T. Saito, D. Kan and Y. Shimakawa, *Chem. Mater.*, 2020, **32**, 8694–8699.
9 M. Zhang, G. Jeerh, P. Zou, R. Lan, M. Wang, H. Wang and S. Tao, *Mater. Today*, 2021, **49**, 351–377.
10 J. Hwang, R. R. Rao, L. Giordano, Y. Katayama, Y. Yu and Y. Shao-Horn, *Science*, 2017, **358**, 751–756.
11 J. Simböck, M. Ghiasi, S. Schönebaum, U. Simon, F. M. F. de Groot and R. Palkovits, *Nat. Commun.*, 2020, **11**, 1–10.
12 W. T. Hong, K. A. Stoerzinger, Y. L. Lee, L. Giordano, A. Grimaud, A. M. Johnson, J. Hwang, E. J. Crumlin, W. Yang and Y. Shao-Horn, *Energy Environ. Sci.*, 2017, **10**, 2190–2200.
13 S. Royer, D. Duprez, F. Can, X. Courtois, C. Batiot-Dupeyrat, S. Laassiri and H. Alamdari, *Chem. Rev.*, 2014, **114**, 10292–10368.
14 M. Jabłońska and R. Palkovits, *Catal. Sci. Technol.*, 2019, **9**, 2057–2077.
15 P. V. B. Santiago, S. P. Raju, K. Akkiraju, S. Yuan, D. Zanchet, Y. Shao-Horn and P. S. Fernández, *Perovskite Oxides as an Opportunity to Systematically Study the Electro-oxidation of Alcohols and Polyols on Materials Based on Abundant Elements: Learning from the Experience Using Pure Metals and Metallic Oxides in (Electro-)Catalysis, n.d*.
16 J. H. White and A. F. Sammells, *J. Electrochem. Soc.*, 1993, **140**, 2167–2177.
17 K. Deshpande, A. Mukasyan and A. Varma, *J. Power Sources*, 2006, **158**, 60–68.
18 A. Lan and A. S. Mukasyan, *J. Phys. Chem. C*, 2007, **111**, 9573–9582.
19 A. C. Brix, M. Dreyer, A. Koul, M. Krebs, A. Rabe, U. Hagemann, S. Varhade, C. Andronescu, M. Behrens, W. Schuhmann and D. M. Morales, *ChemElectroChem*, 2022, **9**, e202200092.
20 P. V. B. Santiago, C. C. Lima, J. L. Bott-Neto, P. S. Fernández, C. A. Angelucci and J. Souza-Garcia, *J. Electroanal. Chem.*, 2021, **896**, 115198.
21 F. Frati, M. O. J. Y. Hunault and F. M. F. De Groot, *Chem. Rev.*, 2020, **120**, 4056–4110.
22 J. Chen, X. Wu and A. Selloni, *Phys. Rev. B*, 2011, **83**, 245204.
23 R. Jacobs, J. Booske, D. Morgan, R. Jacobs, D. Morgan and J. Booske, *Adv. Funct. Mater.*, 2016, **26**, 5471–5482.
24 B. M. Weiss, N. Artioli and E. Iglesia, *ChemCatChem*, 2012, **4**, 1397–1404.
25 R. P. Vasquez, *Surf. Sci. Spectra*, 1992, **1**, 361.
26 M. Krzywiecki, L. Grządziel, A. Sarfraz, D. Iqbal, A. Szwajca and A. Erbe, *Phys. Chem. Chem. Phys.*, 2015, **17**, 10004–10013.
27 W. T. Hong, M. Risch, K. A. Stoerzinger, A. Grimaud, J. Suntivich and Y. Shao-Horn, *Energy Environ. Sci.*, 2015, **8**, 1404–1427.
28 M. E. Abrishami, M. Risch, J. Scholz, V. Roddatis, N. Osterthun and C. Jooss, *Material*, 2016, **9**, 921.
29 J. Suntivich, W. T. Hong, Y. L. Lee, J. M. Rondinelli, W. Yang, J. B. Goodenough, B. Dabrowski, J. W. Freeland and Y. Shao-Horn, *J. Phys. Chem. C*, 2014, **118**, 1856–1863.
30 J. O. Bockris and T. Otagawa, *J. Electrochem. Soc.*, 1984, **131**, 290–302.
31 V. L. Oliveira, C. Morais, K. Servat, T. W. Napporn, P. Olivi, K. B. Kokoh and G. Tremiliosi-Filho, *Electrocatalysis*, 2015, **6**, 447–454.
32 R. N. Singh, T. Sharma, A. Singh, Anindita, D. Mishra and S. K. Tiwari, *Electrochim. Acta*, 2008, **53**, 2322–2330.

33 V. Raghuveer and B. Viswanathan, *Fuel*, 2002, **81**, 2191–2197.
34 V. Raghuveer, K. Ravindranathan Thampi, N. Xanthopoulos, H. J. Mathieu and B. Viswanathan, *Solid State Ionics*, 2001, **140**, 263–274.
35 Z. Yang, Z. Fu, Y. Zhang and R. Wu, *Catal. Lett.*, 2011, **141**, 78–82.
36 H. V. Thang and G. Pacchioni, *Catal. Lett.*, 2019, **149**, 390–398.
37 M. Zeng, X. Wang, Q. Yang, X. Chu, Z. Chen, Z. Li, C. Redshaw, C. Wang, Y. Peng, N. Wang, Y. Zhu and Y. A. Wu, *ACS Appl. Mater. Interfaces*, 2022, **14**, 9882–9890.
38 D. Nandi, V. S. Prabhudesai and E. Krishnakumar, *Phys. Chem. Chem. Phys.*, 2014, **16**, 3955–3963.
39 J. M. D. Tascón and L. G. Tejuca, *J. Chem. Soc., Faraday Trans. 1*, 1981, **77**, 591–602.
40 B. Izadkhah, A. Niaei, M. J. Illán-Gómez, D. Salari, A. Tarjomannejad and V. Albaladejo-Fuentes, *Ind. Eng. Chem. Res.*, 2017, **56**, 3880–3886.
41 L. Forni, C. Oliva, T. Barzetti, E. Selli, A. M. Ezerets and A. V. Vishniakov, *Appl. Catal., B*, 1997, **13**, 35–43.
42 N. Mizuno, M. Tanaka and M. Misono, *J. Chem. Soc., Faraday Trans.*, 1992, **88**, 91–95.
43 J. Suntivich, H. A. Gasteiger, N. Yabuuchi, H. Nakanishi, J. B. Goodenough and Y. Shao-Horn, *Nat. Chem.*, 2011, **3**, 546–550.
44 M. A. Kirsanova, V. D. Okatenko, D. A. Aksyonov, R. P. Forslund, J. T. Mefford, K. J. Stevenson and A. M. Abakumov, *J. Mater. Chem. A*, 2018, **7**, 330–341.
45 J. Hwang, K. Akkiraju, J. Corchado-García and Y. Shao-Horn, *J. Phys. Chem. C*, 2019, **123**, 24469–24476.
46 J. Suntivich, H. A. Gasteiger, N. Yabuuchi, H. Nakanishi, J. B. Goodenough and Y. Shao-Horn, *Nat. Chem.*, 2011, **3**, 546–550.
47 S. C. Sorenson, J. A. Wronkiewicz, L. B. Sis and G. P. Wirtz, *Am. Ceram. Soc. Bull.*, 1974, **53**, 446–449.